

Isospin equilibration in relativistic heavy-ion collisions ^{*} [†]

A. Hombach, W. Cassing and U. Mosel

Institut für Theoretische Physik, Universität Giessen

D-35392 Giessen, Germany

December 2, 2024

Abstract

We study the kinetic and chemical equilibration of projectile and target nucleons in relativistic heavy-ion collisions in the energy regime between 150 A MeV and 2 A GeV in a coupled-channel BUU (CBUU) approach. We find that equilibrium in the projectile-target degrees of freedom is in general not reached even for large systems at low energy where elastic nucleon-nucleon collisions dominate. Inelastic nucleon excitations are more favorable for equilibration and their relative abundance increases both with energy and mass. Experimentally, the projectile/target equilibration can be determined by measuring the degree of isospin equilibration in isospin asymmetric nuclear collisions. For one of the most promising systems currently under investigation, $^{44}_{96}\text{Ru} + ^{40}_{96}\text{Zr}$, we investigate the influence of the equation of state and the inelastic in-medium cross section.

PACS: 25.75. +r

Keywords: Relativistic Heavy-Ion Collisions

^{*}Supported by BMBF and GSI Darmstadt

[†]part of the PhD thesis of A. Hombach

1 Introduction

The aim of relativistic nucleus-nucleus collisions is to produce hot and dense nuclear matter for sufficiently large space-time volumes and to probe the properties of hadrons in a different environment than the vacuum [1, 2, 3, 4, 5, 6]. From particle distributions, spectra and flow one can infer, e. g., on in-medium cross sections and the nuclear equation-of-state (EOS). Experimentally, the properties of the hot and dense part of the system are conventionally described by a temperature T and baryon chemical potential μ_B characterizing the system at freezeout via the relative abundancy or ratio of hadrons [7]. However, if this thermal and chemical equilibrium is actually achieved in the systems studied experimentally is quite a matter of debate [4, 8, 9, 10] and requires an analysis in terms of nonequilibrium transport theory that involves the relevant hadronic degrees of freedom and is applicable in a wide domain of bombarding energies. Experimentally, such equilibration phenomena can be investigated via the isospin degree of degree by using various systems with different N/Z ratios. This technique has been used especially at low bombarding energies (≤ 50 A MeV [11]) and is now being used also at higher energies up to the 1.5 A GeV range at the SIS [8]. For a recent review on the low energy studies we refer the reader to Ref. [12].

In this work we will investigate systematically the degree of isospin equilibration in nucleus-nucleus collisions from 150 A MeV to 2 A GeV. The time evolution of the systems we describe within the coupled-channel BUU (CBUU) transport approach [13] which is briefly described in Section 2. In Section 3 we analyse the dependence on the system mass and beam energy as well as on the centrality of the reaction and compare to related simulations for equilibration phenomena in a finite box with periodic boundary conditions, which allows to determine equilibration times explicitly. Detailed predictions for the total charge ratio for the system $^{44}_{96}\text{Ru} + ^{40}_{96}\text{Zr}$ at 400 A MeV and 1.5 A GeV – which are presently being studied experimentally at the SIS – follow in Section 4 while a summary and a discussion of open problems is given in Section 5.

2 The CBUU-Model

For our present study we employ the CBUU-transport-model [13] to describe the time evolution of relativistic heavy-ion collisions. In this approach, apart from the nucleon, all nucleon resonances up to masses of 1.95 GeV/c² are taken into account as well as the mesons π , η , ρ and σ , where the σ -meson is introduced to describe correlated pion-pairs with total spin $J = 0$. For the baryons as well as for the mesons all isospin degrees of freedom are treated explicitly. The hadrons included in our model obey a set of coupled transport equations for their one-body phase-space distributions $f_i(\vec{r}, \vec{p}, t)$ [14, 15, 16, 17]:

$$\begin{aligned} \frac{\partial f_1}{\partial t} + \left\{ \frac{\vec{p}_1}{E_1} + \vec{\nabla}_p U_1(\vec{r}, \vec{p}_1) \right\} \vec{\nabla}_r f_1 - \vec{\nabla}_r U(\vec{r}, \vec{p}_1) \vec{\nabla}_p f_1 \\ = \sum_{2,3,4} \frac{g}{(2\pi)^3} \int d^3 p_2 \int d^3 p_3 \int d\Omega_4 \delta^3(\vec{p}_1 + \vec{p}_2 - \vec{p}_3 - \vec{p}_4) \\ \times (v_{34} \frac{d\sigma_{34 \rightarrow 12}}{d\Omega} f_3 f_4 \bar{f}_1 \bar{f}_2 - v_{12} \frac{d\sigma_{12 \rightarrow 34}}{d\Omega} f_1 f_2 \bar{f}_3 \bar{f}_4) \quad . \end{aligned} \quad (1)$$

The l.h.s. of eq. (1) represents the relativistic Vlasov-equation for hadrons moving in a momentum-dependent field $U_i(\vec{r}, \vec{p}_i)$ [13], where \vec{r} and \vec{p}_i stand for the spatial and momentum coordinates of the hadrons, respectively. Note, that all space arguments are equal since the collision term in (1) is local. In our model the mesons are propagated as free particles, i.e. $U_i(\vec{r}, \vec{p}_i) \equiv 0$; this has been shown to be a valid approximation at least for π and η mesons [18] whereas the in-medium properties of the ρ -meson are heavily debated [6].

The r.h.s. of eq. (1) describes the changes of $f_i(\vec{r}, \vec{p}_i, t)$ due to two-body collisions among the hadrons and two-body decays of baryonic and mesonic resonances. The in-medium collision rate is represented by $v_{12} \frac{d\sigma_{12 \rightarrow 34}}{d\Omega}$, where σ denotes the free cross section and v_{12} is the relative velocity between the colliding hadrons in their center-of-mass system. The cross sections for the different channels are chosen to reproduce the NN elementary 1π -, 2π -, η and ρ -production cross sections. Taking elastic collisions only, $v_{12} \frac{d\sigma_{12 \rightarrow 34}}{d\Omega}$ equals $v_{34} \frac{d\sigma_{34 \rightarrow 12}}{d\Omega}$; in case of inelastic collisions we factorize the $N+N \rightarrow N+\text{Resonance}$ cross section into (matrix element \times phase space factor) and use these matrix elements for the determination of the backward reaction [19]. For the most important nucleonic resonance, the $\Delta(1232)$, we use a parametrization in line with the result of an OBE model calculation by Dimitriev and Sushkov [20].

In eq. (1), $\bar{f}_i = 1 - f_i$ ($i = 1, \dots, 4$) are the Pauli-blocking factors for fermions. In

the collision integrals describing two-body decays of resonances one has to replace the product (relative velocity \times cross-section $\times f_2$) by the corresponding decay rate and introduce the proper fermion blocking factors in the final channel. The factor g in (1) stands for the spin degeneracy of the particles participating in the collision whereas $\sum_{2,3,4}$ stands for the sum over the isospin degrees of freedom of particles 2, 3 and 4.

We include the following elastic and inelastic baryon-baryon, meson-baryon collisions and meson-meson collisions:

$$\begin{aligned}
NN &\longleftrightarrow NN \\
NN &\longleftrightarrow NR \\
NR &\longleftrightarrow NR' \\
NN &\longleftrightarrow \Delta(1232)\Delta(1232) \\
R &\longleftrightarrow N\pi \\
R &\longleftrightarrow N\pi\pi \\
&= \Delta(1232)\pi, N(1440)\pi, N\rho, N\sigma \\
N(1535) &\longleftrightarrow N\eta \\
NN &\longleftrightarrow NN\pi \\
\rho &\longleftrightarrow \pi\pi \quad (\text{p-wave}) \\
\sigma &\longleftrightarrow \pi\pi \quad (\text{s-wave}), \tag{2}
\end{aligned}$$

where R and R' represent the baryonic resonances [13]. For the $NN \rightarrow \Delta(1232)\Delta(1232)$ reaction we use the parametrization of Huber and Aichelin [21]; $NN \rightarrow NN\pi$ is an s-wave contribution to the total pion production cross section below the Delta resonance.

The mean field U entering the l.h.s. of eq. (1) is of the MDYI-type as proposed by Welke et al. [22, 23, 24]

$$U(\vec{r}, \vec{p}) = A \frac{\rho(\vec{r})}{\rho_0} + B \frac{\rho(\vec{r})^\tau}{\rho_0} + 2 \frac{C}{\rho_0} \int d^3p' \frac{f(\vec{r}, \vec{p}')}{1 + \left(\frac{\vec{p}-\vec{p}'}{\Lambda}\right)^2}. \tag{3}$$

This ansatz enables to guarantee energy conservation since it can be derived from a potential energy density functional. The parameters of the potential U are chosen to match the requirements

$$\frac{E}{A}|_{\rho_0} = -16 \text{ MeV}, \quad \frac{\partial E}{\partial \rho}|_{\rho_0} = 0, \quad K = 210|260|380 \text{ MeV},$$

$$U(E = 300 \text{ MeV}) = 0 \quad \text{and} \quad U(p = \infty) = +32 \text{ MeV} \quad . \quad (4)$$

These constraints we derive from the results of the microscopic calculations by Wiringa et al. [25, 26] with Hamiltonians required to describe NN scattering data, few body binding energies and nuclear matter saturation properties. Best agreement to [26] over the whole density regime of 0.1 to 0.5 fm⁻³ would be achieved using a compressibility $K \simeq 230 \text{ MeV}$, however, we fit the three different compressibilities denoted in (4) as soft, medium and hard equation of state (EOS). Additionally, we introduce an asymmetry potential U_{sym} , depending only on the densities of protons and neutrons

$$U_{\text{sym}} = D \frac{\rho_p - \rho_n}{\rho_0} \tau_z \quad , \quad (5)$$

with $D = 30 \text{ MeV}$ and $\tau_z = \pm 1$ for protons and neutrons, respectively. With the help of this potential we are able to reproduce the isospin and mass dependence of the binding energy of nuclei correctly [27]. However, we find the effects of different binding energy and asymmetry potential to be negligible for the energy range ($E/A \geq 400 \text{ MeV}$) considered here.

The baryons and mesons are represented by testparticles and eq. (1) is solved numerically in the parallel ensemble algorithm. The particles are propagated according to

$$\begin{aligned} \frac{d\vec{r}_i(t)}{dt} &= \frac{\vec{p}_i}{E_i} + \vec{\nabla}_p U(\vec{r}_i, \vec{p}_i(t)) \\ \frac{d\vec{p}_i(t)}{dt} &= -\vec{\nabla}_r U(\vec{r}_i, \vec{p}_i(t)) - q_i \vec{\nabla} V_C(\vec{r}_i), \end{aligned} \quad (6)$$

whereas for collisions $b < b_{\text{max}} = \sqrt{\sigma/\pi}$ is required in addition to $b = \text{minimal}$ in the current timestep [28].

This model has been shown to adequately describe pion spectra [13], pion multiplicities [19] as well as Coulomb effects on charged pion spectra [29].

3 Equilibration in heavy-ion collisions

Within the CBUU model outlined in the previous section we first investigate the isospin equilibration as a function of the system size and incident energy. Later we will focus on the difference between the 'true' equilibration in the center of the reaction and the experimentally accessible signal which is affected also by surface

effects and reaction centrality. Note, that the term 'equilibration' in this paper is used in a different meaning than e. g. in thermal equilibrium; equilibrium means the total isotropy of the baryonic isospin distribution here. This charge isotropy is thought to be synonymous to a total admixture of target and projectile nucleons.

We have chosen $^{28}_{58}\text{Ni} + ^{28}_{58}\text{Ni}$ (with a total mass number of 116) as a representative for a lighter system and $^{79}_{197}\text{Au} + ^{79}_{197}\text{Au}$ (with a total mass number of 394) as a heavy system. The experimentally investigated combination $^{44}_{96}\text{Ru} + ^{40}_{96}\text{Zr}$ [8] which we refer to with its total mass number of 192 is inbetween these two and will be considered in section 4. As the combinations Ni+Ni and Au+Au consist of reaction partners of equal isospin, we will directly use the normalized ratio of target over projectile nucleons as a measure for the isospin mixture of the system. Note, that in the transport approach each hadron trajectory can be traced back to the incident projectile and target and thus isospin equilibration can be analysed in the full phase space at every time.

For relative comparison we will also perform calculations in a finite box with periodic boundary conditions using two shifted Fermi spheres with given N/Z ratio as initial condition. The relative momentum shift and N/Z ratio is uniquely determined by the projectile-target combination and bombarding energy, respectively. These "infinite nuclear matter" studies allow to investigate the time scales for kinetic and chemical equilibration for times $t \rightarrow \infty$, whereas any heavy-ion reaction is limited by the total interaction time.

3.1 Mass and energy dependence

Fig. 1 shows the rapidity distribution in the final state of a central Au+Au collision at 150 AMeV. Though the total rapidity spectrum dN/dy is close to that of a thermal distribution [9], here compared to a calculation in a box with periodic boundary conditions and $\rho \simeq \rho_0$ for $t \rightarrow \infty$, the rapidity distributions of target and projectile nucleons are still clearly separated in the 'free' collision (in the following we will use the expression 'free' collision for realistic simulations of nucleus-nucleus collisions) within our semiclassical phase-space simulation. This separation of projectile and target nucleons will approximately persist in a fully quantum-mechanical treatment of the reaction dynamics since only about 1/4 of the NN collisions occur between pairs of identical particles (same spin and isospin) which cannot be distinguished

in the final state due to the Pauli principle. However, taken as approximation for isospin equilibration the distributions in Fig. 1 show clearly that equilibration is not reached in this reaction. This "transparency" is also supported e.g. by the longitudinally elongated event topologies for $Z = 3$ fragments as shown in Ref. [9].

We now consider – in order to exclude surface effects – a tube around the beam axis of radius $r=1$ fm and calculate for each rapidity bin of typically $0.2 \times y_0$ (where y_0 denotes the cms rapidity normalized to the projectile rapidity in this system) the number of projectile minus target nucleons and normalize it to the total number of nucleons in this bin. The resulting ratio then varies between +1 for having only projectile nucleons in one bin and -1 for target nucleons, respectively, and is a direct measure for the degree of isospin or target/projectile mixing in the system.

This target/projectile ratio is shown in Fig. 2 for central Au+Au collisions at different kinetic energies. As already indicated in Fig. 1, the ratio is clearly different from zero at low energies. Above about 400 AMeV the Au+Au system begins to equilibrate and shows even a repulsion of target and projectile matter at 2 AGeV. A very similar behaviour is found for the Ni+Ni system in Fig. 3, besides the fact that this lighter system never fully admixes. At projectile rapidity the number of projectile nucleons always exceeds the number of target nucleons. This is due to the lower size of the fireball which limits the number of inelastic collisions and is too small for an equilibration of the Ni+Ni system.

In order to investigate the influence of the size and temperature of the fireball on equilibration in more detail we have calculated the equilibration ratio as function of time for systems in a box with periodic boundary conditions as described above. We compare these calculations to the time available for equilibration during the lifetime of the fireball in a 'free' collision. The box was chosen such that the minimum density lies between 0.7 and $1 \times \rho_0$. As a global equilibration ratio we have averaged the individual ratios in each rapidity bin over all rapidities from -0.9 to $0.9y_0$. The 'free' fireball lifetimes to compare with we define as the time interval from the rise of the density in the center of the reaction zone above ρ_0 to the drop below $0.5\rho_0$ in a 'free' collision. This corresponds to the time period in which practically all NN-collisions in a HIC happen as indicated by Fig. 4.

The results for both Au+Au and Ni+Ni are shown in Fig. 5. All global ratios start from zero (since there are no particles in the rapidity interval $-0.9 < y < 0.9$ initially) and reach a maximum between 5 and 10 fm/c. The maximum possible

value of the global ratio is 19. Defining equilibration by the ratio $\leq 10\%$ of the maximum, clearly the time needed to equilibrate is much longer than the lifetime of the fireball at 150 and 400 AMeV for both systems. On the other hand, equilibration is reached for $^{79}_{197}\text{Au} + ^{79}_{197}\text{Au}$ at 1 AGeV but not for $^{28}_{58}\text{Ni} + ^{28}_{58}\text{Ni}$ at this energy. At 2 AGeV a negative ratio is observed between $t=8$ and 15 fm/c, which is due to the strong repulsion of the target and projectile matter in the dense reaction zone. Since matter can not escape to the side due to the boundary conditions imposed, a shock front runs from the collision zone in opposite direction to the instreaming matter thus inverting their average direction of motion. Less pronounced this happens also in a 'free' reaction as reflected by the negative ratio at 2 AGeV in Figs. 2 and 3.

In summarizing this section, we like to point out that the main limiting factor for achieving projectile-target equilibration in the energy region of 150 AMeV to 2 AGeV is the number of *inelastic* NN-collisions per volume that occur throughout a HIC. This collision number is again limited by the lifetime of the fireball, given by the size of the system, and the incident energy of the collision. We find the decrease with bombarding energy to be stronger than the increase of the overall reaction time when going to lower bombarding energies. On the other hand, the relative influence of the nucleon potential increases with decreasing energy. Here especially the momentum dependence gives some additional stopping for the relative motion between target and projectile as compared to a pure cascade or a density dependent (Skyrme) potential. However, even at 150 AMeV the collisions play the dominant role for stopping.

3.2 Surface effects and dependence on centrality

In the previous section we have considered the 'true' mixture of the system by taking a tube around the beam axis, thus excluding any surface effects. Experimentally, however, only an overall equilibration is measurable and one has to consider the influence of corona effects, which means that the surfaces of the colliding nuclei pass each other. Additionally, the results measured will be affected by dominant contributions from non-central collisions where spectator matter will spoil the signal of equilibration in the fireball. So the ability to determine central events will be a crucial point experimentally. In the following we will therefore investigate both the effects of surface contributions as well as criteria for centrality selection on the signal

for the Au+Au system, for which we could extensively check the agreement of our results on multiplicity, transverse energy and directivity distributions to experimental data at various energies [9, 30].

Fig. 6 shows the target to projectile ratio defined in the last section for central, $b=1$ fm and $b=2$ fm collisions in comparison to the 'true' ratio along the beam axis, determined in the cylinder geometry as explained in the previous section. The $b=0$ overall ratio is, besides a difference at high rapidities, in very good agreement to the true ratio; for $b=1$ fm the agreement is still acceptable. Surface effects contribute mainly at $y > y_{pr}$ and are negligible for rapidities below $0.9y_0$. However, the centrality selection is crucial since already the $b=2$ fm results differ substantially from the 'true' signal. Since higher impact parameters enter in an impact parameter integrated measurement with higher statistical weight, we have checked on experimental possibilities to suppress these.

A usual way to determine central events is given by selecting events with a high transverse energy to longitudinal energy ratio E_{rat} ,

$$E_{\text{rat}} = \frac{\sum_i (p_x^2 + p_y^2)}{\sum_i p_z^2} , \quad (7)$$

and applying additional cuts in directivity

$$D = \frac{|\sum \vec{p}_t|}{\sum |\vec{p}_t|} , y > y_{cm} , \quad (8)$$

where the usual FOPI-Cuts of $7^\circ \leq \Theta_{\text{lab}} \leq 30^\circ$ have to be used.

Fig. 7 shows the experimental E_{rat} distribution for Au+Au at 400 AMeV in comparison to the CBUU calculations. Additionally, the CBUU distributions obtained for $b=0.1$, $b=1$ and $b=2$ runs are shown separately. The distributions of the individual impact parameters are very broad and especially the $b=2$ fm impact parameter still contributes substantially at high E_{rat} . Thus for an event sample with $E_{\text{rat}} > 1.2$ we have applied additional cuts in directivity, ranging from $D < 0.02$ to $D < 0.3$. The relative contributions of runs at different impact parameters are shown in Fig. 8. It can clearly be seen that requiring a narrow cut in D is an excellent way to select central events, though contributions from $b=2$ fm runs cannot be completely excluded. The latter we cannot quantify exactly due to statistical uncertainties caused by the low number of events surviving these strong cuts.

However, the systems should be taken as massive as possible since corona effects increase with decreasing mass. For the Au+Au system investigated in this subsection

they are negligible. Beyond this, when requiring sufficiently low directivity D , it should be possible experimentally to exclude non-central events and to measure a signal very close to the 'true' target–projectile mixture as discussed in the previous section.

4 The Ru+Zr system

Experimentally projectile and target nucleons are indistinguishable. In order to gain information on the degree of equilibration one can choose projectile – target combinations of different isospin and evaluate the uniformness of the isospin distribution at different rapidities. Experiments are currently under consideration at the SIS, where measurements with $^{44}_{96}\text{Ru}$ and $^{40}_{96}\text{Zr}$ at 400 AMeV and at 1.5 AGeV are being investigated.

The system Ru+Zr with a total mass number of 192 behaves more similar to the Ni+Ni system than to Au+Au as shown in Fig. 9. For this system we have also first determined the target over projectile ratio since this quantity is, first of all, numerically much more stable and, second, direct proportional to the isospin ratio. For the two energies mentioned above, we have investigated the factors influencing the mixing ratio and the dependence on varying these. The results are shown in Fig. 10. At 400 AMeV (l.h.s.) we find the incompressibility K of the equation of state (EOS) to be the dominant factor, even though the dependence is not very strong. Close to the Ni+Ni system discussed in section 3.1, in the Ru+Zr system the number of inelastic collisions is much too low at 400 AMeV for equilibration thus giving rise to a target/projectile ratio up to 0.6 at projectile rapidities. By increasing the compressibility one decreases the number of collisions even more; this leads to an increase of the ratio and vice versa. Note that when varying the inelastic cross section within reasonable limits ($\pm 30\%$) negligible effects are found in this energy regime which is essentially dominated by elastic processes.

At 1.5 AGeV the situation is different. Though an overall equilibration is again not reached here due to the small number of collisions limited by the size and lifetime of the fireball, the target to projectile ratio is close to zero up to normalized rapidities $y_0 \simeq 0.6$ and reaches its maximum value of 0.4 at y_{pr} . The incompressibility of nuclear matter plays a minor role at these energies, whereas a variation of the inelastic cross section changes the degree of equilibration by $\approx 10\%$. So in principle

it could be possible to determine in-medium cross sections and the EOS separately by looking at the isospin equilibration at different energies and system sizes.

For the charge or isospin ratio one has to consider the shift of the total baryonic isospin due to charged pion production at higher energies. In order to normalize the p/n-ratio vs. rapidity to ± 1 for $^{44}_{96}\text{Ru}$ and $^{40}_{96}\text{Zr}$, respectively, one has not to take the initial isospin ratios of ~ 0.85 for Ru and ~ 0.71 for Zr but the final ones given by $\frac{44 - \sum \pi^+}{96 - 44 - \sum \pi^-}$ and $\frac{40 - \sum \pi^+}{96 - 40 - \sum \pi^-}$ for Ru and Zr, being approximately 0.90 and 0.81 in our calculation at 1.5 AGeV. The statistical uncertainties of our calculation on the isospin ratio – given not only by the number of particles in each rapidity bin but also by the statistical uncertainty of the charged pion number – are shown in Fig. 11. These fluctuations blur the difference between the 400 AMeV and the 1.5 AGeV curve shown in Fig. 12, which should closely follow the respective lines in Fig. 10. However, experimentally it should be possible to determine the charge ratios with sufficient accuracy.

5 Summary

In this paper we have explored the possibility to determine the degree of target/projectile equilibration via the measurement of isospin ratios vs. rapidity in the final state of HIC's of isospin asymmetric systems. The analysis has been performed within the coupled-channel (CBUU) transport approach which has proven in Refs. [13, 29] to adequately describe pion spectra as well as baryon flow in the SIS energy regime [31]. In our calculations the isospin dependence of both the inelastic and elastic scattering cross section is taken into account, as well as an isospin dependent mean-field potential. However, in the energy range considered here the influence of the isospin asymmetric potential term is negligible as well as a separate consideration of Pauli blocking for protons and neutrons.

We find that full equilibration is practically never achieved even in central collisions of Au + Au. This is due to the fact that elastic collisions at lower energy (≤ 400 AMeV) are not very effective for baryon stopping due to forward peaked angular distributions. Inelastic baryon excitations help very much for equilibration such that central Au+Au collisions at 1 AGeV show an approximate equilibration. This is due to the fact that the lifetime of the fireball is sufficiently long as compared to an equilibration time evaluated for a related infinite nuclear matter

problem within the CBUU approach. For Ni+Ni we find no full equilibration at all bombarding energies considered here.

We have shown explicitly the influence of surface effects and examined criteria for centrality selection on the equilibration signature. As result, it should be possible, when selecting central events carefully, to achieve experimentally a signal at least close to the 'true' equilibration of the system, i.e. the equilibrium in that region where the centers of the colliding nuclei are located.

In addition, it has been shown that the incompressibility K of the EOS modifies the signal at lower energies somewhat, whereas medium modifications of the cross section dominantly influence the signal at high bombarding energy. Thus in principle it might be possible to determine the EOS and the medium modifications of the inelastic cross section independently by N/Z ratios vs. rapidity in very central collisions of different systems at e.g. 400 AMeV and 1.5 AGeV. For a determination of the EOS light systems should be used since the short lifetime of the fireball limits the number of inelastic collisions. One promising system could be $^{48}\text{Ca}+^{50}\text{Cr}$ as proposed in [4]. On the other hand, the determination of changes in the in-medium cross section does not require very heavy systems in the mass region of $^{79}_{197}\text{Au}+^{79}_{197}\text{Au}$. These equilibrate anyhow in the energy regime of ≈ 1 AGeV and thus are insensitive to minor changes ($\pm 30\%$) of the inelastic cross section. In this sense the Ru+Zr system is promising in yielding results limiting both the variety of the compressibility of the EOS and the in-medium cross sections.

References

- [1] H. Stöcker and W. Greiner, Phys. Rep. **137** (1986) 277.
- [2] W. Cassing and U. Mosel, Prog. Part. Nucl. Phys. **25** (1990)235.
- [3] J. Aichelin, Phys. Rep. **202** (1991) 233.
- [4] S. Bass et al., nucl-th/9803035, Prog. Part. Nucl. Phys. (1998), in print
- [5] C. M. Ko and G. Q. Li, J. Phys. G: Nucl. Part. Phys. **22** (1996) 1673.
- [6] W. Cassing and E. L. Bratkovskaya, Phys. Rep. (1998), in press

- [7] P. Braun-Munzinger, J. Stachel, J. P. Wessels, and N. Xu, Phys. Lett. **B 344** (1995) 43; **B 365** (1996) 1.
- [8] Y. Leifels et al., GSI report 1/98 (1998) 57.
- [9] W. Reisdorf et al., Nucl. Phys. **A 612** (1997) 493.
- [10] W. Reisdorf, Nucl. Phys. **A 630** (1998) 15c.
- [11] J. F. Dempsey et al., Phys. Rev. **C 54** (1996) 1710.
G. J. Kunde et al., Phys. Rev. Lett. **77** (1996) 2897.
- [12] B. A. Li, C. M. Ko and W. Bauer, Int. J. Mod. Phys. **E 7** (1998) 147.
- [13] S. Teis, W. Cassing, M. Effenberger, A. Hombach, U. Mosel and Gy. Wolf, Z. Phys. **A 356** (1997) 421.
- [14] G. F. Bertsch and S. Das Gupta, Phys. Rep. **160** (1988) 189.
- [15] W. Cassing, K. Niita and S.J. Wang, Z. Phys. **A 331** (1988) 439.
- [16] W. Cassing, V. Metag, U. Mosel and K. Niita, Phys. Rep **188** (1990) 363.
- [17] K. Weber, B. Blättel, W. Cassing, H.-C. Dönges, V. Koch, A. Lang, and U. Mosel, Nucl. Phys. **A 539** (1992) 713; K. Weber, B. Blättel, W. Cassing, H.-C. Dönges, A. Lang, T. Maruyama and U. Mosel, Nucl. Phys. **A 552** (1993) 571
- [18] E. L. Bratkovskaya, W. Cassing, R. Rapp, and J. Wambach, Nucl. Phys. **A 634** (1998) 168.
- [19] S. Teis, PhD Thesis, University of Giessen 1996.
- [20] V. Dimitriev and O. Sushkov, Nucl. Phys. **A 459** (1986) 503.
- [21] S. Huber and J. Aichelin, Nucl. Phys. **A 573** (1994) 587.
- [22] G. M. Welke, M. Prakash, T. T. S. Kuo and S. Das Gupta, Phys. Rev. **C 38** (1988) 2101.
- [23] C. Gale, G. M. Welke, M. Prakash, S. J. Lee and S. Das Gupta, Phys. Rev. **C 41** (1990) 1545.
- [24] J. Zhang, S. Das Gupta and C. Gale, Phys. Rev. **C 50** (1994) 1617.

- [25] R. B. Wiringa and V. Fiks, Phys. Rev. **C 38** (1988) 1010.
- [26] R. B. Wiringa, Phys. Rev. **C 38** (1988) 2967.
- [27] Th. Weidmann, E. L. Bratkovskaya, W. Cassing and U. Mosel, submitted to Phys. Rev. C., nucl-th/9711004.
- [28] T. Kodama et al., Phys. Rev. **C 29** (1984) 2146.
- [29] S. Teis, W. Cassing, M. Effenberger, A. Hombach, U. Mosel and Gy. Wolf, Z. Phys. **A 359** (1997) 297.
- [30] Th. Wienold, PhD Thesis, GSI report 7/93.
- [31] P. K. Sahu, A. Hombach, W. Cassing, U. Mosel, and M. Effenberger, Nucl. Phys. A, in press.

Figure captions

Fig. 1: Baryon rapidity distribution of a central 150 AMeV $Au + Au$ collision (solid line) in comparison to the thermal equilibrium rapidity distribution as calculated in a box with periodic boundary conditions (squares). For the central collision the rapidity distributions of projectile nucleons (dashed) and target nucleons (dotted) are displayed separately.

Fig. 2: Ratio of target to projectile nucleons in a tube along the beam direction as defined in section 3.1 as a function of rapidity for central $Au + Au$ collisions at different bombarding energies. For 150, 400 and 2000 AMeV error bars are given to indicate the statistical uncertainty of the result.

Fig. 3: Same as Fig. 2 for the $Ni + Ni$ system.

Fig. 4: Evolution of the density in the center of the reaction zone (solid line) and the collision rate (dotted line) in a central $Au + Au$ collision at 2 AGeV. The vertical dashed lines indicate the boundaries of the time interval available for equilibration as given by the onset of the collisions and the drop of the central density below $0.5\rho_0$.

Fig. 5: Global equilibrium ratio as a function of time for systems evolving in a box with periodic boundary conditions; $Au + Au$ (l.h.s.) and $Ni + Ni$ (r.h.s.) in comparison to the fireball lifetimes of the corresponding 'free' collision (vertical dotted lines).

Fig. 6: Comparison between the "true" equilibrium in a tube along the z-axis (excluding surface effects) (solid line) and the overall equilibrium for $b=0, 1$ and 2 fm collisions (dashed, dash-dot and dotted line, respectively) for $Au + Au$ at 0.4 AGeV.

Fig. 7: The distribution in E_{rat} for $Au + Au$ at 400 AMeV. The experimental data (squares) have been taken from [9] while the CBUU results are given by the dotted line. Also shown are the individual distributions for $b=0.1, 1$ and 2 fm collisions from the CBUU calculations (solid, dashed and dash-dotted line).

Fig. 8: Contributions to different directivity bins of an event sample with $E_{\text{rat}} > 1.2$

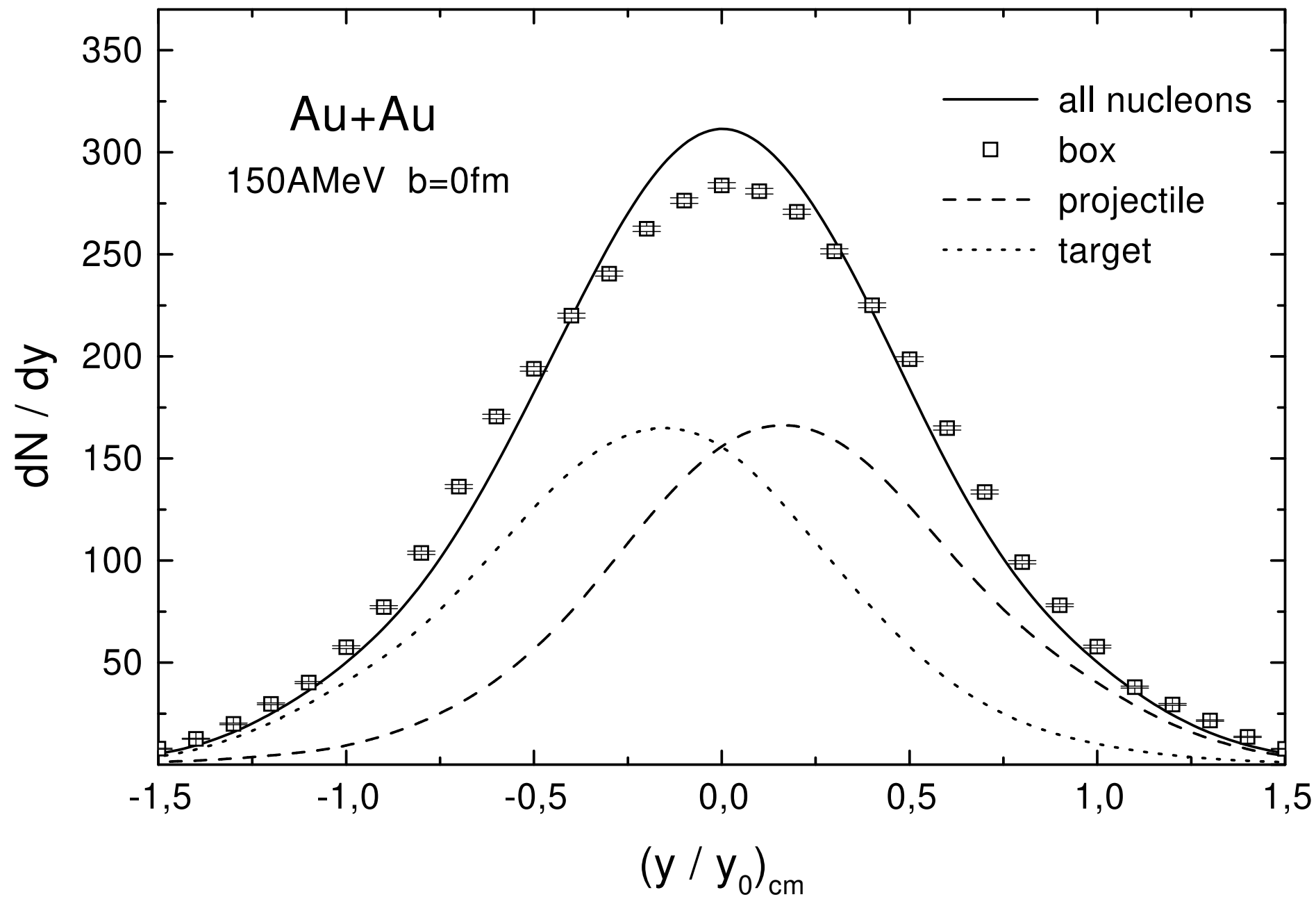
for $Au + Au$ at 400 AMeV.

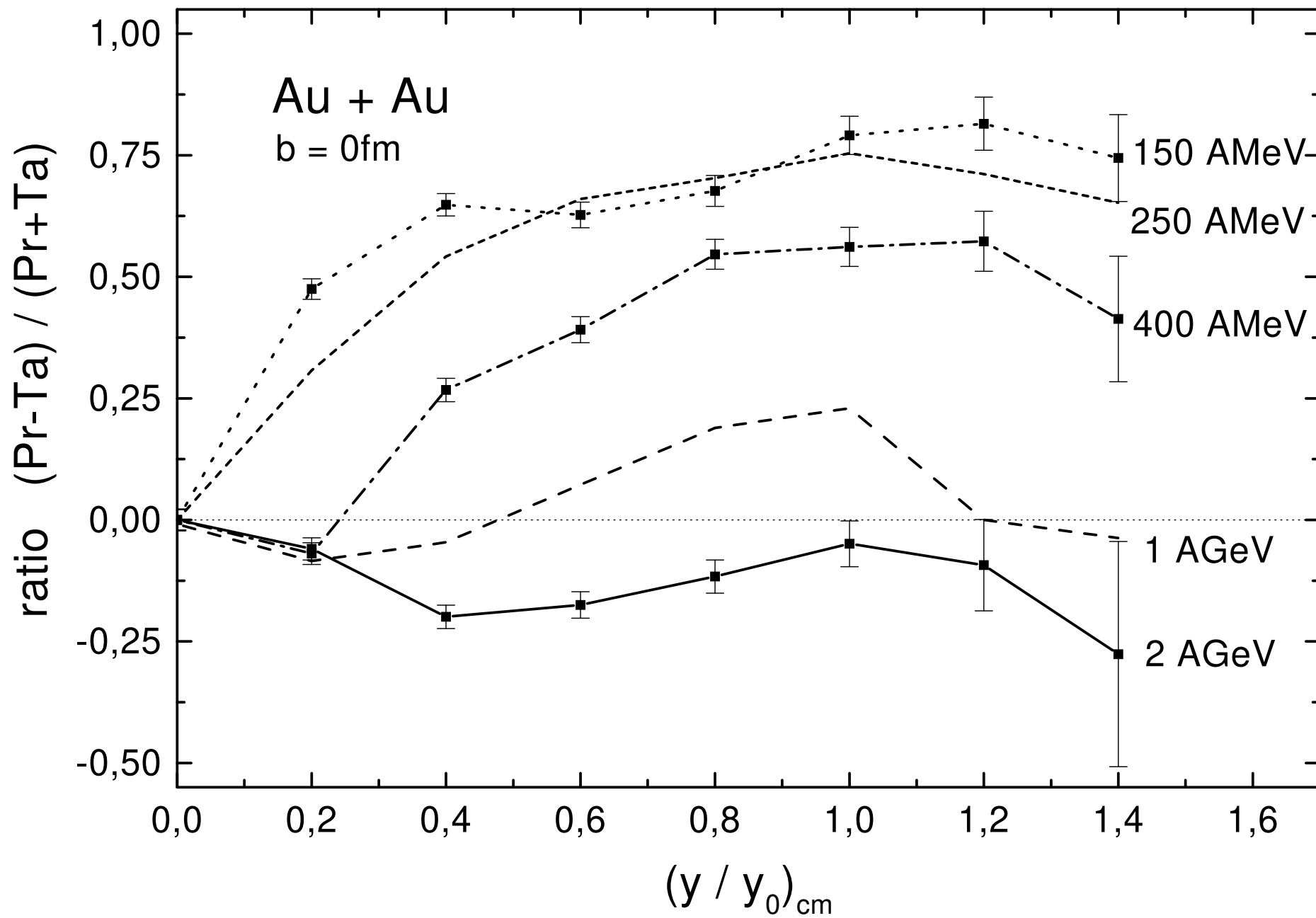
Fig. 9: Mass dependence of the target-projectile mixture. Shown are target to projectile ratios vs. rapidity for $Au+Au$ (dashed), $Ru+Zr$ (solid) and $Ni+Ni$ (dotted).

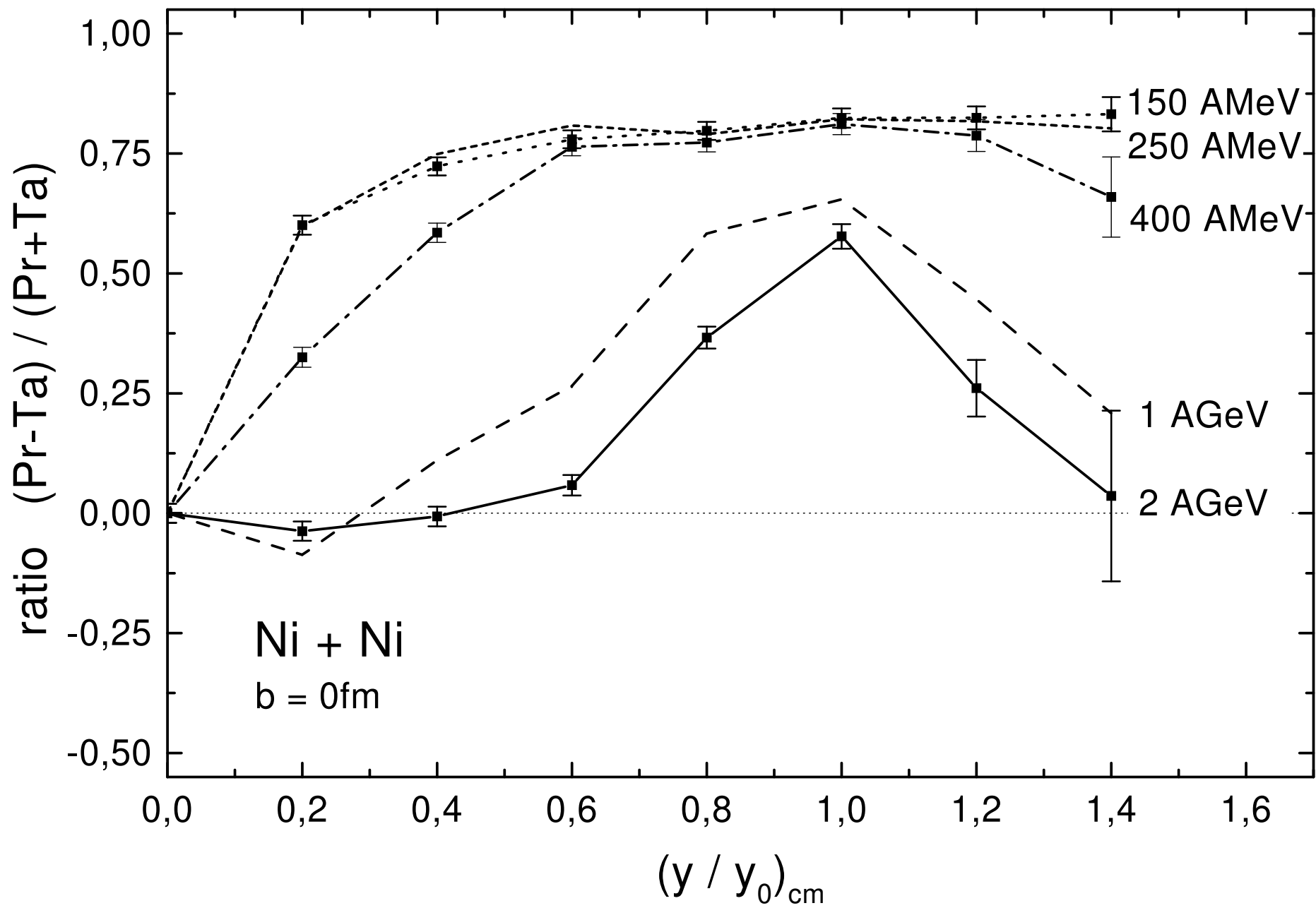
Fig. 10: Target to projectile ratio for the $Ru + Zr$ system for different energies of 400 AMeV (l.h.s.) and 1500 AMeV (r.h.s.). The upper plots show the influence of different equations of state while in the lower plots the in-medium inelastic cross section is varied by $\pm 30\%$.

Fig. 11: Charge ratios vs. rapidity for $Ru + Ru$ (solid lines) and $Zr + Zr$ (dashed lines) collisions at 400 AMeV (upper panel) and 1500 AMeV (lower panel).

Fig. 12: Charge ratios vs. rapidity for $Zr + Ru$ collisions at 400 AMeV (solid line) and 1500 AMeV (dashed line).







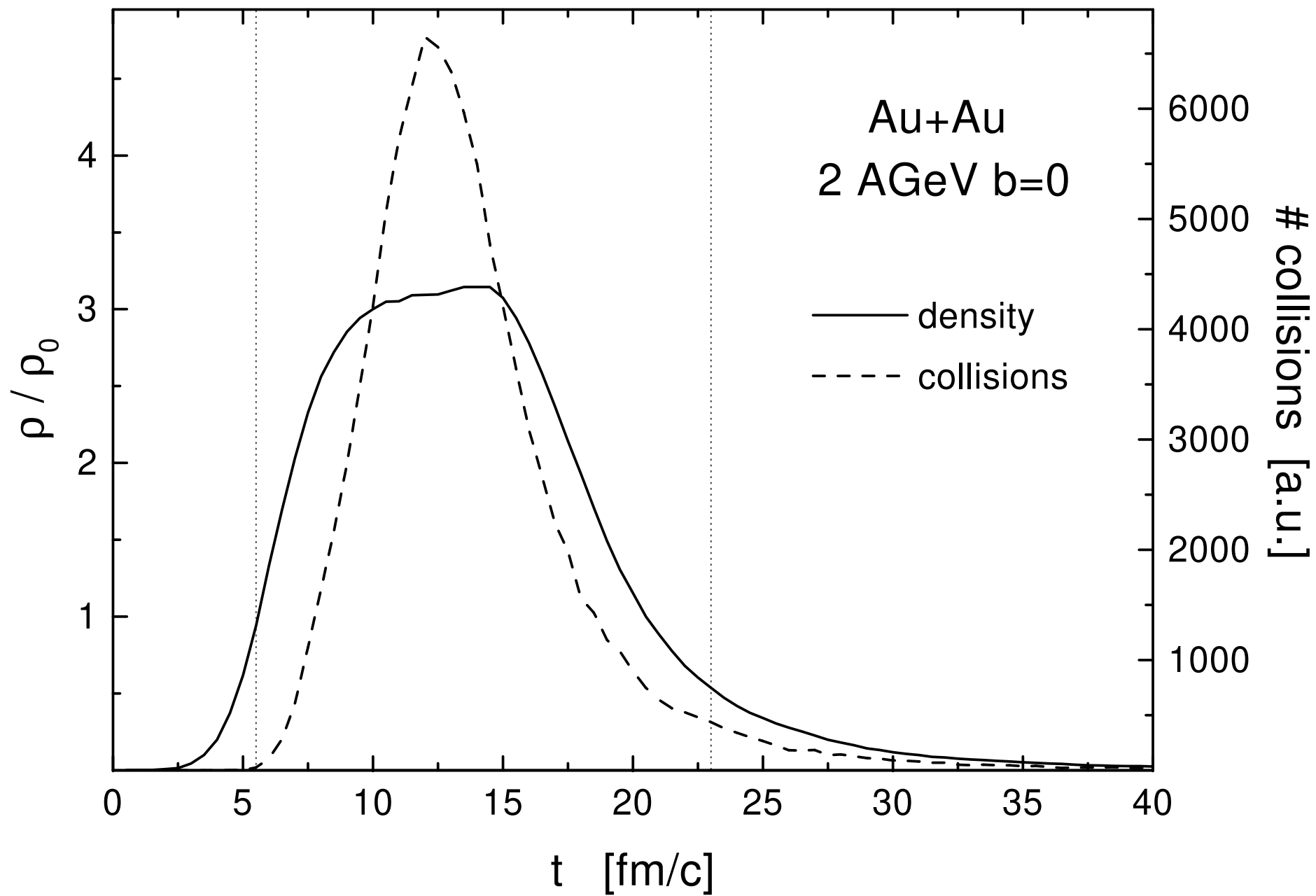
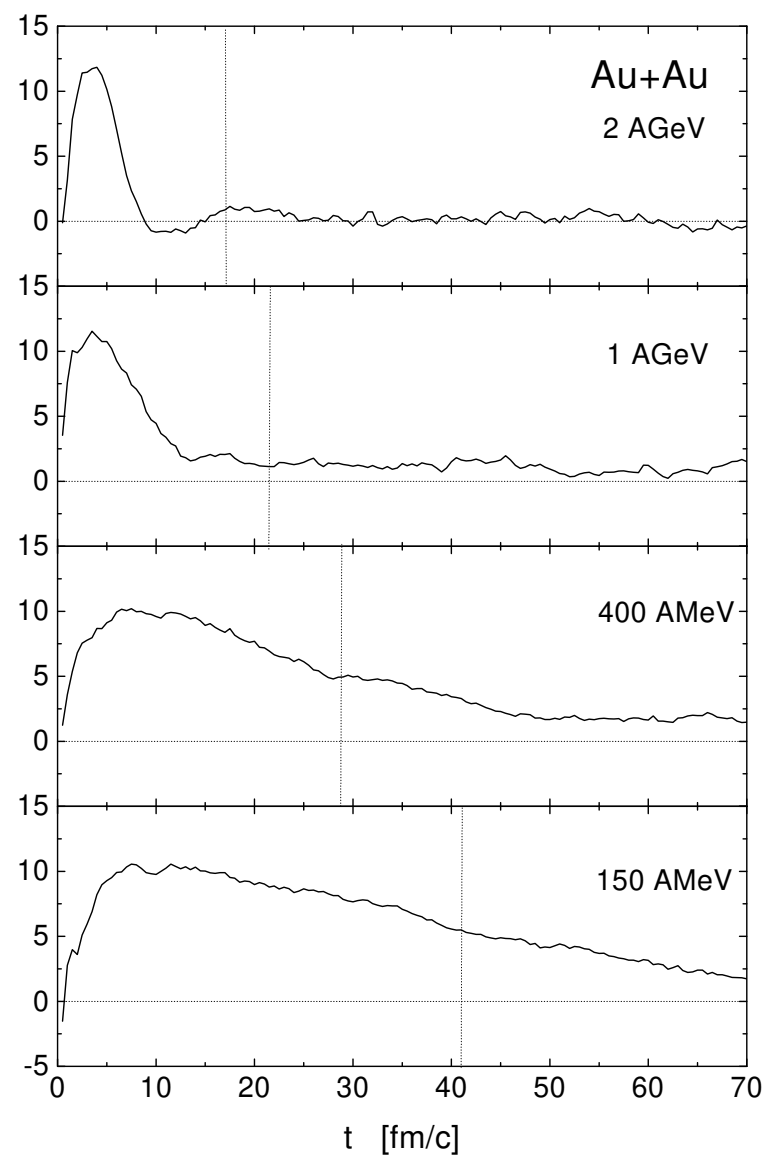
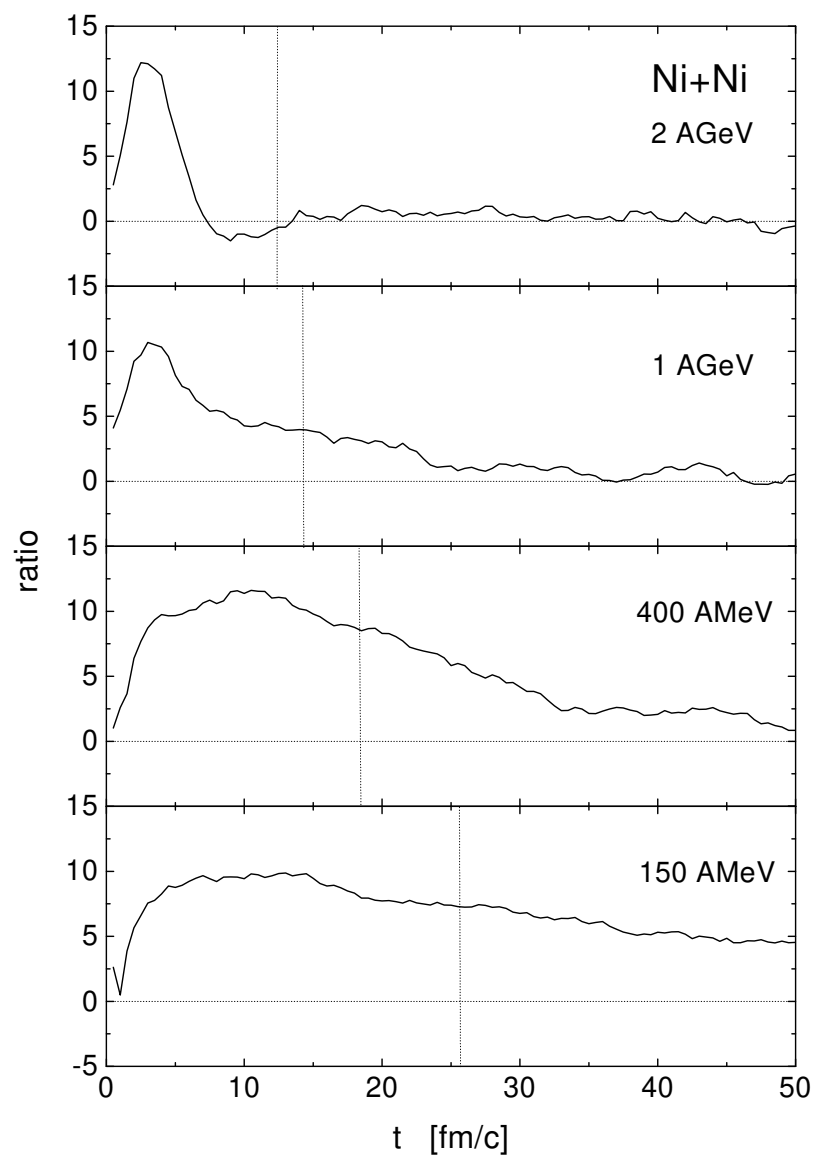
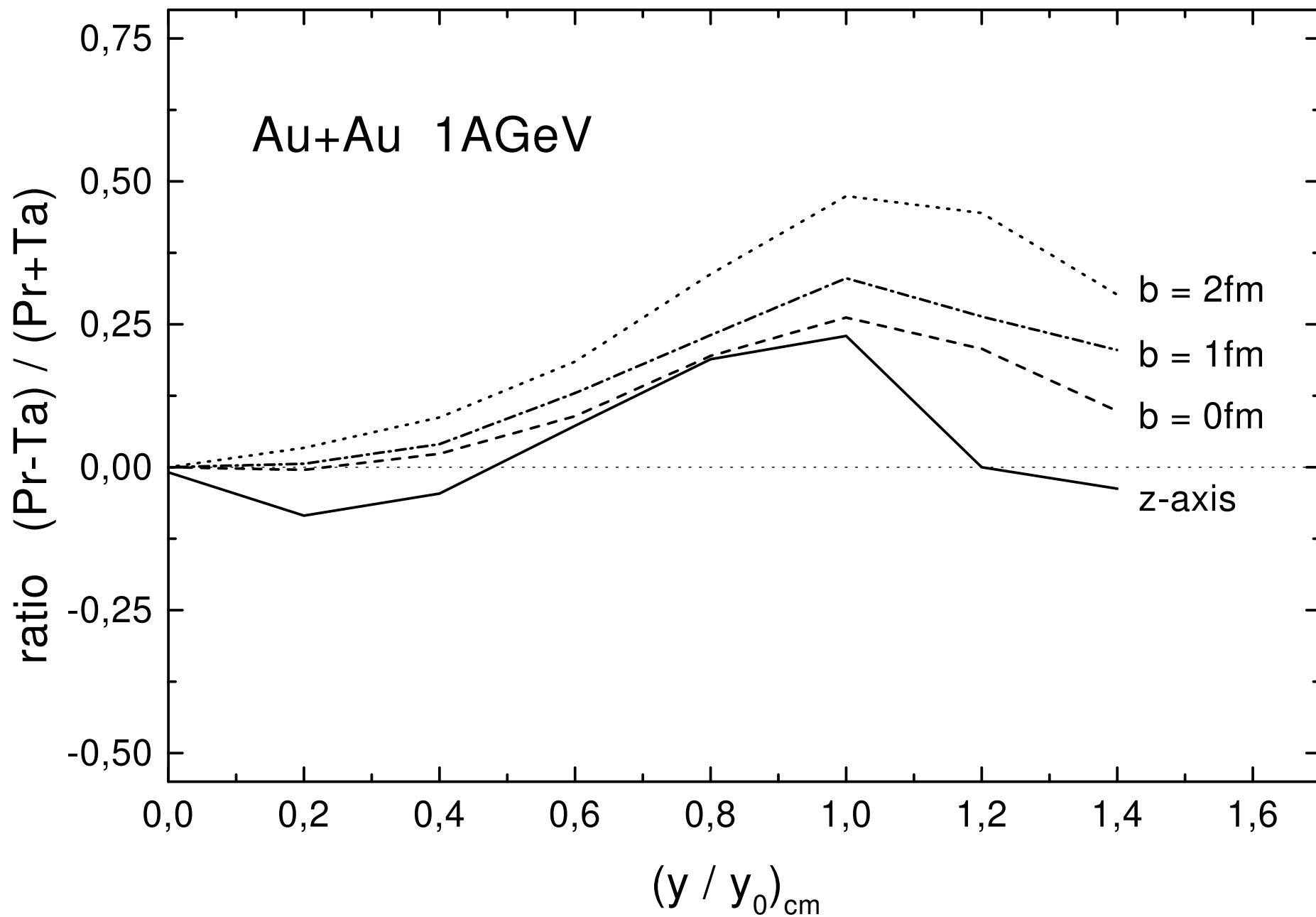
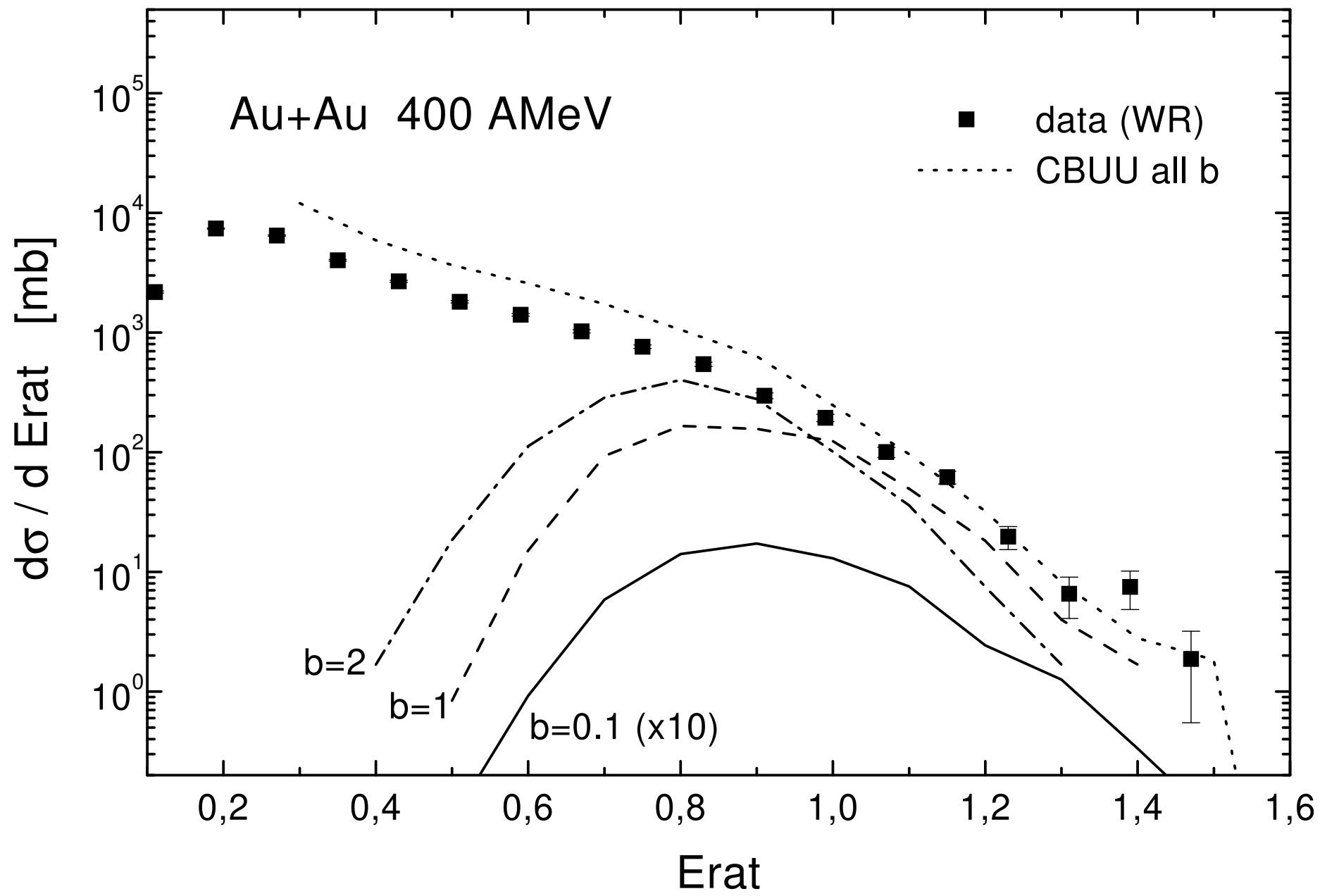
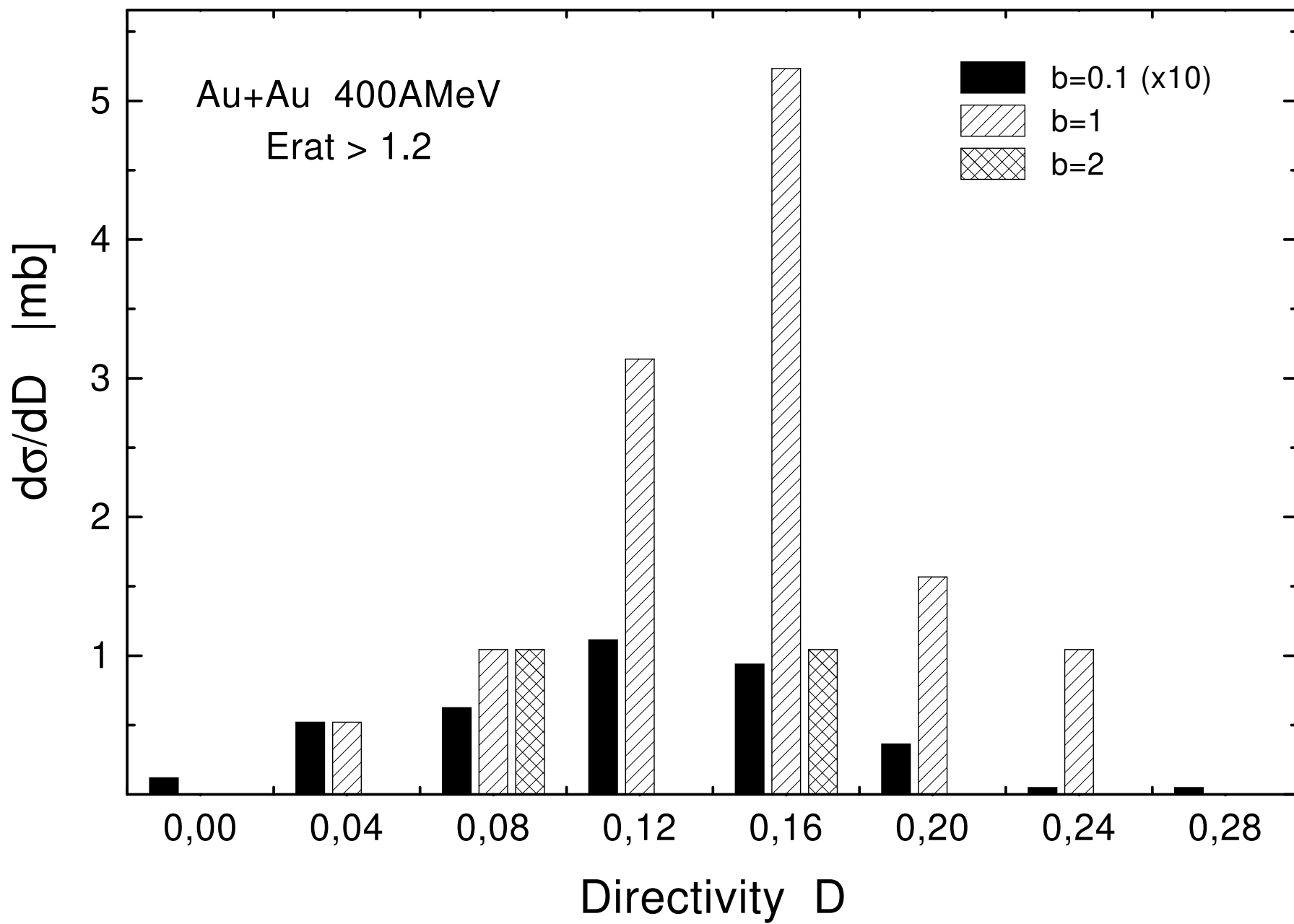


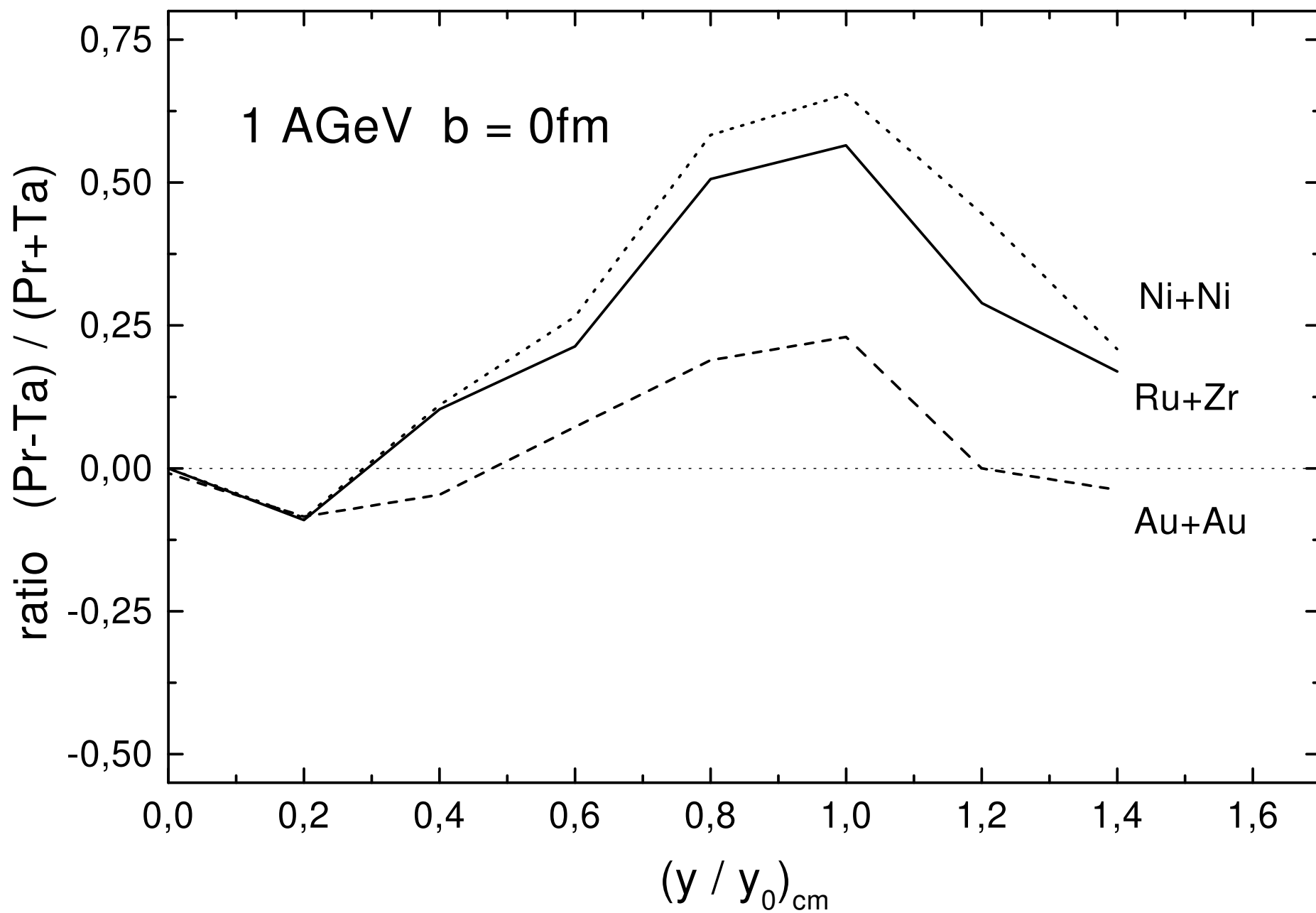
Figure 5:

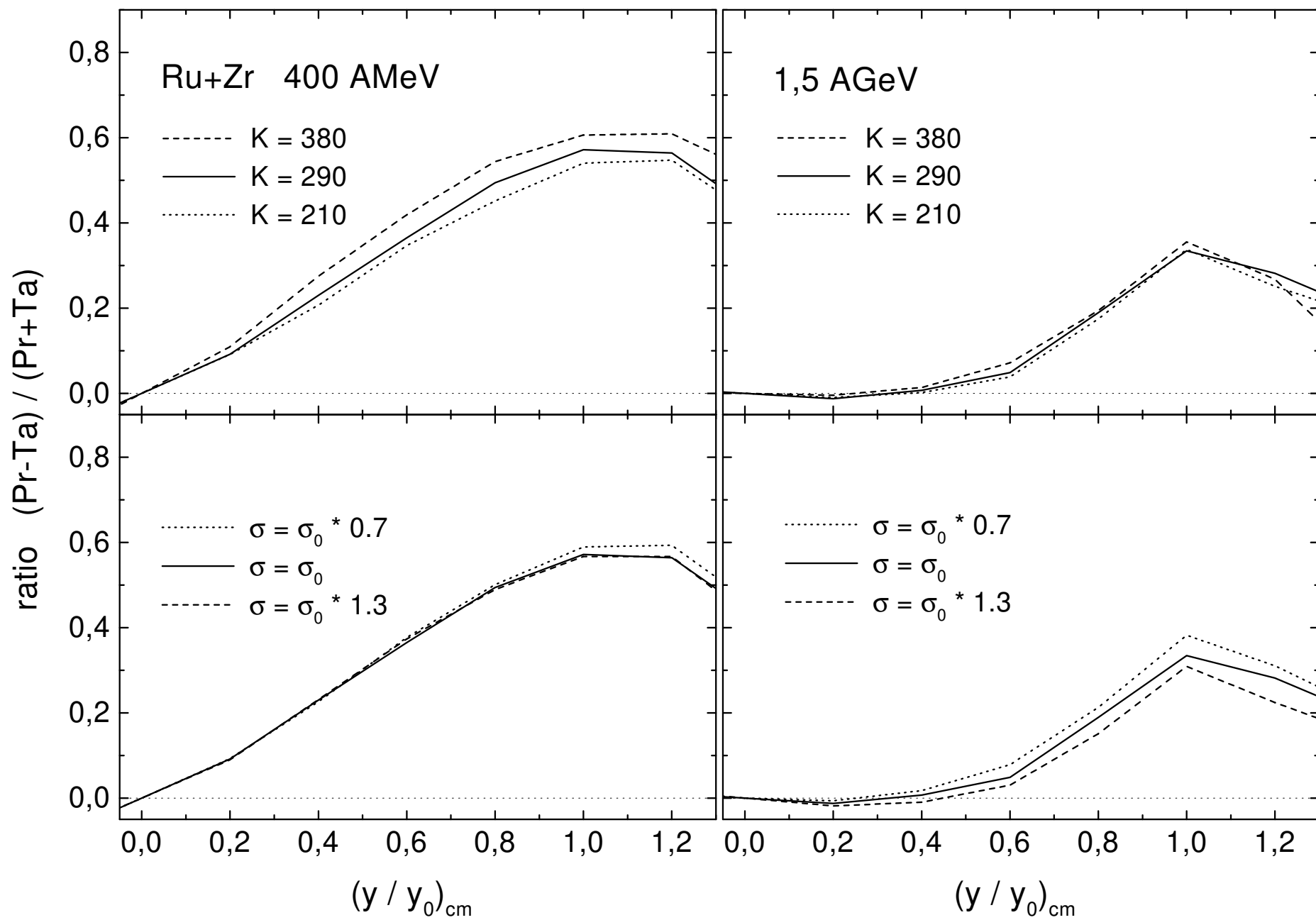












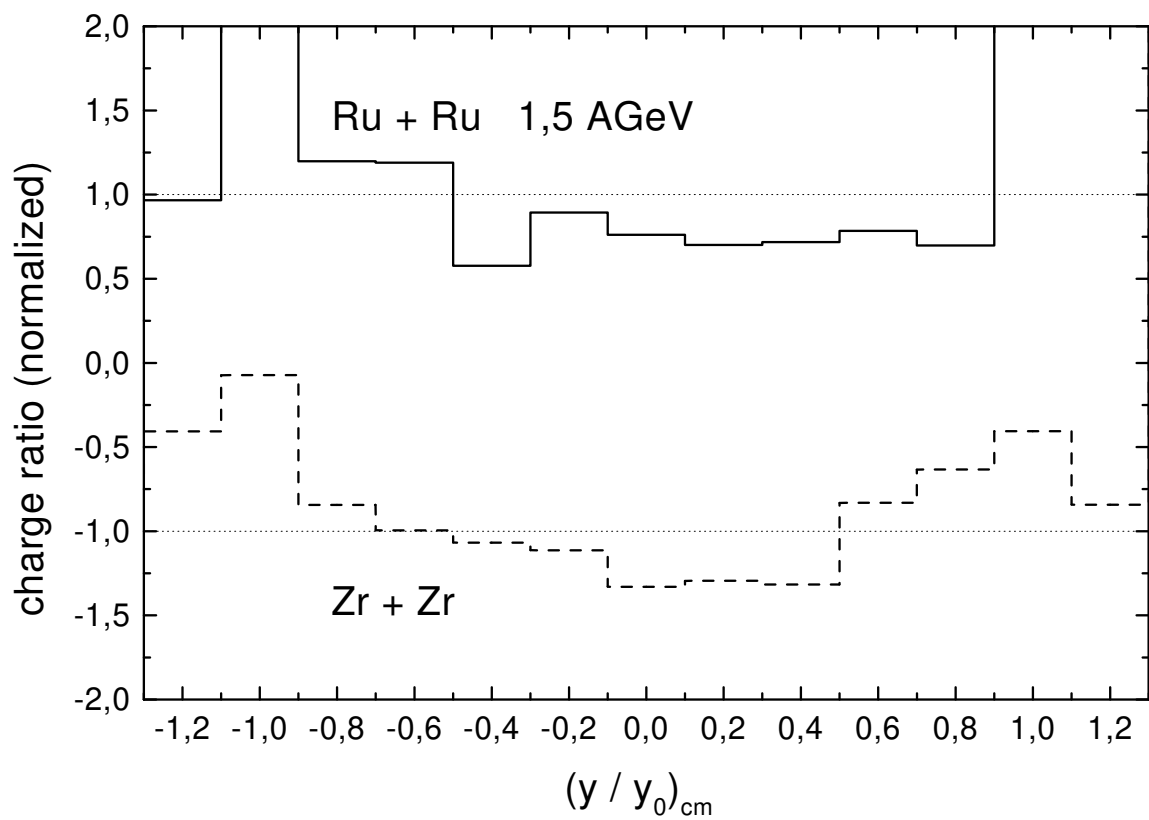
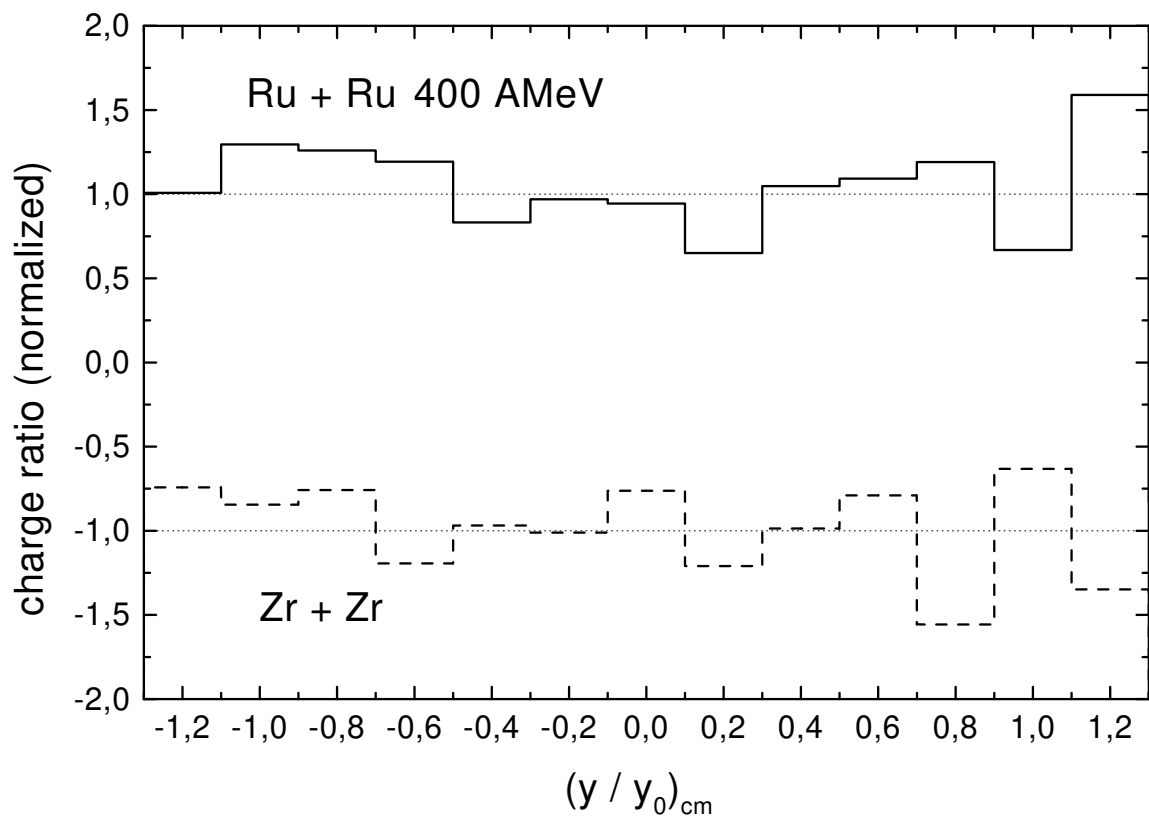


Figure 11:

